

Delayed use of bioenergy crops might threaten climate and food security

<https://doi.org/10.1038/s41586-022-05055-8>

Received: 27 October 2021

Accepted: 29 June 2022

Published online: 7 September 2022

 Check for updates

Siqing Xu¹, Rong Wang^{1,2,3,4,5,6}✉, Thomas Gasser⁷, Philippe Ciais^{8,9}, Josep Peñuelas^{10,11}, Yves Balkanski⁸, Olivier Boucher¹², Ivan A. Janssens¹³, Jordi Sardans^{10,11}, James H. Clark^{1,14}, Junji Cao¹⁵, Xiaofan Xing¹, Jianmin Chen^{1,2,3}, Lin Wang^{1,2,3}, Xu Tang^{2,3} & Renhe Zhang^{2,3,4,5}

The potential of mitigation actions to limit global warming within 2 °C (ref. ¹) might rely on the abundant supply of biomass for large-scale bioenergy with carbon capture and storage (BECCS) that is assumed to scale up markedly in the future^{2–5}. However, the detrimental effects of climate change on crop yields may reduce the capacity of BECCS and threaten food security^{6–8}, thus creating an unrecognized positive feedback loop on global warming. We quantified the strength of this feedback by implementing the responses of crop yields to increases in growing-season temperature, atmospheric CO₂ concentration and intensity of nitrogen (N) fertilization in a compact Earth system model⁹. Exceeding a threshold of climate change would cause transformative changes in social–ecological systems by jeopardizing climate stability and threatening food security. If global mitigation alongside large-scale BECCS is delayed to 2060 when global warming exceeds about 2.5 °C, then the yields of agricultural residues for BECCS would be too low to meet the Paris goal of 2 °C by 2200. This risk of failure is amplified by the sustained demand for food, leading to an expansion of cropland or intensification of N fertilization to compensate for climate-induced yield losses. Our findings thereby reinforce the urgency of early mitigation, preferably by 2040, to avoid irreversible climate change and serious food crises unless other negative-emission technologies become available in the near future to compensate for the reduced capacity of BECCS.

One hundred and ninety-one parties responsible for 97% of global anthropogenic greenhouse gas (GHG) emissions have joined the Paris Agreement, with the objective to limit global warming by this century to 2 °C while pursuing efforts to stay within warming of 1.5 °C (ref. ¹). Global warming in 2021 is approaching 1.2 °C above the 1850–1900 average². Achieving all pledges under the nationally determined contributions may limit warming to just below 2 °C, which requires steep emissions reductions in the current decade¹⁰. Many mitigation scenarios nonetheless assume that climate change could be mitigated by negative-emission technologies such as BECCS, which would be deployed in the second half of this century to benefit from technological advances^{3–5}. However, large-scale deployment of BECCS faces biophysical, technical and social challenges^{11,12}. An over-reliance on BECCS could delay other decarbonizing technologies and fail to meet the Paris goal under overshoot scenarios¹³. Early actions are important to avoid irreversible climate change and pronounced shifts in land use¹⁴. The USA, the European Union and China, the three largest emitters of carbon dioxide (CO₂), aim to achieve carbon (C) neutrality by either

2050 or 2060 (ref. ¹). The effectiveness of these pledges depends largely on the remaining emissions in countries that have not yet made such pledges and on feedbacks in the carbon–climate systems¹⁵ that have not been fully recognized by current integrated assessment models (IAMs)².

Climate change is projected to be decelerated by strongly abating CO₂ emissions from fossil fuels¹⁰, but large-scale negative-emission technologies at a global scale are required in most of the scenarios limiting global warming to 2 °C (ref. ²). Retrofitting coal-fired power plants to BECCS, which substitutes fossil fuels by generating electricity with biomass from lignocellulosic energy crops or residues and removes CO₂ from the atmosphere, is assumed to be a cost-effective option in IAMs^{16,17}. Capturing CO₂ from the combustion of agricultural residues from food crops (such as maize and rice) or dedicated energy crops and storing it in geological sites are proposed to achieve the 2 or 1.5 °C target in the sixth assessments of the Intergovernmental Panel on Climate Change (IPCC)². Using the biomass from agricultural residues as feedstocks to generate electricity is more economical than growing dedicated energy crops (such as *Miscanthus*)^{18,19}. Because the population and food

¹Shanghai Key Laboratory of Atmospheric Particle Pollution and Prevention (LAP³), Department of Environmental Science and Engineering, Fudan University, Shanghai, China. ²IRDR International Center of Excellence on Risk Interconnectivity and Governance on Weather/Climate Extremes Impact and Public Health, Fudan University, Shanghai, China. ³Institute of Atmospheric Sciences, Fudan University, Shanghai, China. ⁴Shanghai Frontiers Science Center of Atmosphere–Ocean Interaction, Shanghai, China. ⁵MOE Laboratory for National Development and Intelligent Governance, Fudan University, Shanghai, China. ⁶Institute of Eco-Chongming (IEC), Shanghai, China. ⁷International Institute for Applied Systems Analysis (IIASA), Laxenburg, Austria. ⁸Laboratoire des Sciences du Climat et de l'Environnement, CEA CNRS UVSQ, Gif-sur-Yvette, France. ⁹Climate and Atmosphere Research Center (CARE-C), The Cyprus Institute, Nicosia, Cyprus. ¹⁰CSIC, Global Ecology Unit CREAF-CSIC-UAB, Bellaterra, Spain. ¹¹CREAF, Cerdanyola del Vallès, Spain. ¹²Institut Pierre-Simon Laplace, Sorbonne Université/CNRS, Paris, France. ¹³Department of Biology, University of Antwerp, Wilrijk, Belgium. ¹⁴Green Chemistry Centre of Excellence, University of York, York, UK. ¹⁵Institute of Atmospheric Physics, Chinese Academy of Sciences, Beijing, China. ✉e-mail: rongwang@fudan.edu.cn

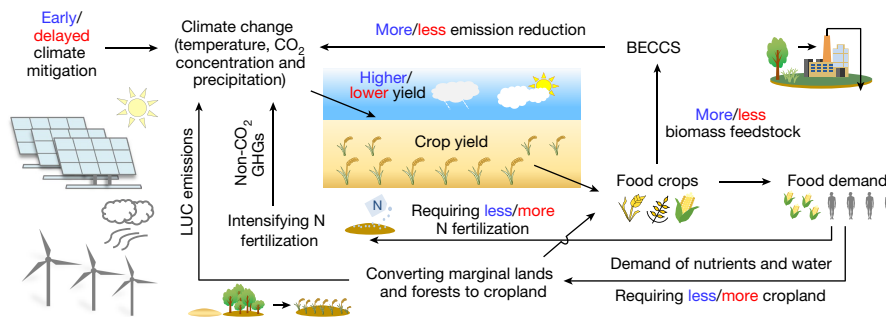


Fig. 1 | Climate–yield feedbacks owing to reduced biomass feedstocks of crop residues for BECCS and the potential impacts on food supply and LUC. This illustration shows the response of a social–ecological system relying on

agricultural residues for bioenergy to a delay of mitigation with large-scale BECCS (from blue to red).

demand from developing countries are both increasing²⁰, transferring residues of agricultural crops to BECCS would reduce the competition of new dedicated energy crops with food production for resources such as land, fertilizers and water²¹. Future crop yields, however, may decline owing to the detrimental effects of climate warming^{6–8} if strong mitigation actions are delayed, thereby reducing the capacity of BECCS for mitigation (Fig. 1). These feedbacks have not been considered in current IAMs^{2–4}, which rely on the availability of agricultural residues¹⁸ or dedicated energy crops⁵ for BECCS at a large scale. The impacts of BECCS on the food–climate–energy nexus have been assessed in the literature (Supplementary Table 1), but the feedbacks of reduced BECCS capacity to climate warming are unclear. Further measures such as irrigation²², adaptation of crop cultivars²³ and conservation agriculture⁸ are helpful for increasing the productivity of cropland, but the widespread water scarcity owing to the increasing frequency and intensity of droughts around the globe²⁴ may limit the potential of those adaptation measures for increasing crop yields. A quantification of the impact of reduced crop yields on climate change mitigation is needed for estimating the interactions between biological and techno-economic components²⁵ of the Earth system, recognizing the tipping points in social–ecological systems²⁶ and assessing the effectiveness of emission pledges to meet the 2 °C goal in the Paris Agreement¹.

Scenarios of climate mitigation with BECCS

We examined how the benefits of ambitious mitigation with large-scale BECCS aimed at meeting climate and food targets could be offset owing to reduction in crop yields under climate change (Fig. 1). We quantified the impact of climate change on crop yields in a set of scenarios in which global large-scale mitigation is initiated at the start of each decade from 2030 to 2100. When ambitious mitigation starts, we assumed that policy reduces fossil emissions from the baseline scenario of the Shared Socioeconomic Pathway (SSP) 5–8.5 to the lower-emission scenario of SSP2–4.5 (ref. ²) while BECCS is deployed using agricultural residues globally (Supplementary Fig. 1 and Methods). There are other decarbonizing technologies taking place from 2030 to meet emission pledges in the SSP2–4.5 scenario, but they imply a lack of negative emissions to be compliant with net-zero emissions² by 2100. SSP5–8.5 is worse than what seems to be ‘business-as-usual’ emissions²⁷, but phasing out fossil fuels rapidly and deploying BECCS moves our projections close to the IPCC low-warming scenarios². Cumulative emissions during 2021–2050 in our scenario with mitigation starting in 2030 are 380 Gt C from fossil fuel reduction alone, with further negative emissions of –120 Gt C from BECCS by 2050 (Supplementary Fig. 2). These net emissions (260 Gt C) are higher than SSP1–1.9 (150 Gt C) but similar to SSP1–2.6 (250 Gt C)², which meets the Paris goal of 2 °C (ref. ¹).

In our assumptions, the area of land converted from forests or marginal lands to cropland and the intensity of N fertilization depend on

the food demand in 2030 (for example, a higher food demand elicits more land conversion from forests or marginal lands to cropland). The impacts of transferring C associated with land-use change (LUC) from soils and vegetation to the atmosphere, and of the terrestrial emissions of methane and nitrous oxide (N₂O) on climate change, were simulated using the OSCAR Earth system model⁹. We estimated the average growing-season temperature for maize, rice and wheat by country based on global crop calendar data (Methods). We considered a scenario in which half of cropland expansions from forests and marginal lands²⁸ were used to grow new energy crops and the other half were used to grow food crops with the residues used for BECCS. Because technologies increase crop yields, we considered two scenarios: (1) the N use efficiency would be enhanced globally²⁹ and (2) the growing season was brought forward or delayed by one month to increase the crop yield by country. Negative emissions from BECCS were estimated on the basis of the amount of C produced as biomass and an efficiency of capturing 90% of the CO₂ emitted by BECCS plants³⁰, while we examined the climate benefits for different types of bioenergy. Interactions between climate change and the global C cycle have been calibrated using the results of models in Coupled Model Intercomparison Project (CMIP)³¹ Phase 5 and Phase 6. By running Monte Carlo simulations with OSCAR⁹, our results are representative of the CMIP ensembles³¹ and the variation in the yield–climate relationships.

Relationships between crop yields and climate

We estimated the relationships between crop yields (*Y*) and the average growing-season temperature (T_{atm}), atmospheric CO₂ concentration (X_{CO_2}) and N fertilization (Z_{nit}) using global data. First, crop yield peaks at an optimal temperature (T_{opt}) and decreases when temperatures increase beyond T_{opt} owing to increasing water loss by evapotranspiration and lower enzymatic activity in foliar photosynthesis when T_{atm} exceeds a criterion^{7,32} (Fig. 2a,b). In our central case, we used a quadratic function to fit the yields of wheat and maize from field-warming experiments and local process-based or statistical crop models (Supplementary Table 2 and Supplementary Data Set 1) by constraining T_{opt} (Supplementary Table 3). We considered that the yield of wheat would be reduced to 1% of its maximum value when T_{atm} exceeded 29 °C (T_{dam})³³ to represent the effect of heat exposure over the whole growing season. Short exposures to temperatures above 40 °C with low humidity may be lethal³⁴, but the effect of extreme heat events is not considered owing to the lack of direct evidence. Following this, we examined the impact of increasing T_{opt} or T_{dam} by 1 °C or using data from field-warming experiments only, which altered the $Y–T_{atm}$ function moderately (Supplementary Fig. 3). We examined the linear or non-linear $Y–T_{atm}$ functions to fit the sensitivity of wheat yield to temperature for $T_{atm} \leq 15$ °C from field-warming experiments⁷, which led to a faster decline in crop yield for $T_{atm} < 25$ °C than our estimate (Supplementary Fig. 3).

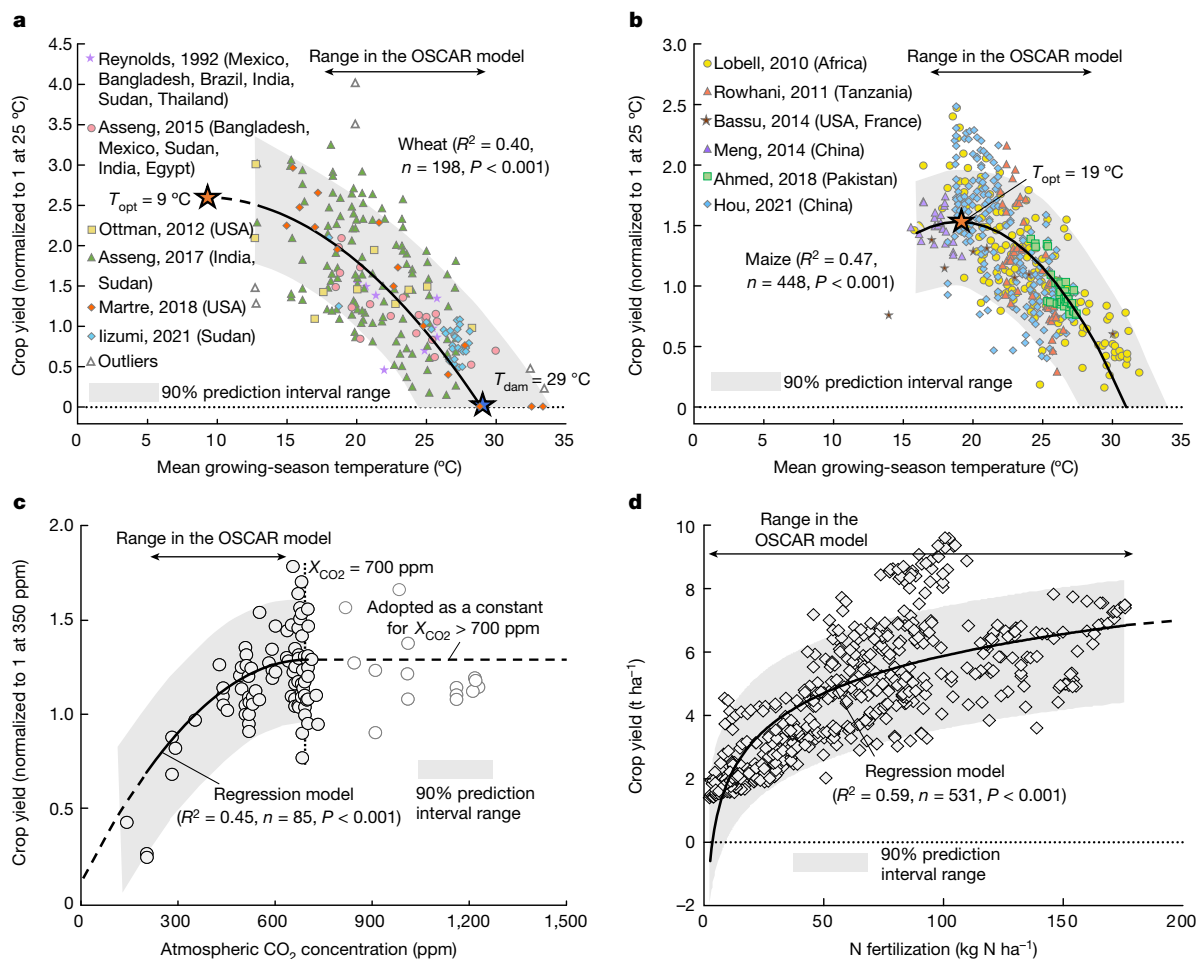


Fig. 2 | Relationships between crop yield, climate and land management.

a, b, A quadratic function of average growing-season atmospheric temperature (T_{atm} , $^\circ\text{C}$) is used to fit the yields of wheat (**a**) and maize (**b**). The yields are derived from field-warming experiments and process-based or statistical models from 13 countries worldwide (Supplementary Table 2), in which the yields are normalized to 1 at $25\text{ }^\circ\text{C}$ for different studies. Six outliers are excluded ($P < 0.005$). We adopted the optimal temperature (T_{opt}) for maize ($19\text{ }^\circ\text{C}$) and wheat ($9\text{ }^\circ\text{C}$) as an average in different countries or regions (Supplementary Table 3) and assumed that the yield is reduced to 1% of its maximum value when T_{atm} exceeds $29\text{ }^\circ\text{C}$ (T_{dam})^{33,34}. We used the yield (Y)–temperature functions fit to the local data to predict the crop yields by country if applicable and applied the functions fit to global data in the remaining

Second, elevated X_{CO_2} increases the rate of plant photosynthesis of C_3 crops and the yields of wheat and rice³⁵. This effect saturates when X_{CO_2} exceeds 700 ppm (Fig. 2c), probably owing to the co-limitation of soil nutrients and water³⁶. We used a quadratic function to fit the saturating yield of wheat grown with ample water and nutrients at an optimal temperature in free-air CO_2 -enrichment experiments³⁷ for $X_{CO_2} < 700\text{ ppm}$ ($P < 0.001$) and assumed a flat response for $X_{CO_2} > 700\text{ ppm}$. This empirical sensitivity of Y to X_{CO_2} is similar to the sensitivity obtained with crop models for wheat in the Netherlands and rice in Japan, but is larger for maize as a C_4 crop in Tanzania that is exposed to higher temperatures³⁸ (Supplementary Fig. 3). Third, N addition is beneficial for the growth of crops, but the effect decreases with excessive inputs³⁹. We used a logarithmic function to fit the yields of rice, wheat, maize and soybeans⁴⁰ by region from 1961 to 2019 after adjusting for the impacts of T_{atm} , X_{CO_2} and precipitation (Fig. 2d and Supplementary Fig. 4). The yield of rice increases sixfold when N fertilization increases from 5 to 100 kg ha^{-1} but only by 12% when it increases further from 100 to 150 kg ha^{-1} .

regions of the world. The shaded area shows the 90% interval range of the fitted function, which is adopted in our Monte Carlo simulations. **c**, A quadratic function of atmospheric CO_2 concentration (X_{CO_2}) is used to fit the wheat yield³⁷ for $X_{CO_2} < 700\text{ ppm}$. The yields are normalized to 1 at 350 ppm . A constant yield is predicted for $X_{CO_2} \geq 700\text{ ppm}$, at which the correlation between Y and X_{CO_2} is not significant ($P = 0.16$). **d**, A logarithmic function of N fertilization (Z_{nit}) is used to fit the yield of rice as an example (see Supplementary Fig. 4 for the yields of wheat, maize and soybeans)⁴⁰ in the nine regions of the OSCAR model from 1961 to 2019. The yields in **d** have been adjusted for the impacts of T_{atm} , X_{CO_2} and precipitation (Methods). The data used to fit the functions are listed in Supplementary Data Set 1. The arrow in each panel shows the range of T_{atm} , X_{CO_2} or Z_{nit} in the OSCAR model.

The yield–climate relationships are compared among five agriculturally important countries (Supplementary Fig. 5). Crop yield is more sensitive to warming at lower latitudes and more sensitive to N inputs in the USA than in other countries³⁸. We assumed that the dependencies of crop yield on air temperature, CO_2 concentration and N fertilization for a limited set of species could be generalized to energy crops owing to the lack of consistent data for those specific cultivars. We adopted the parameters calibrated in a previous study⁹ to prescribe regional responses of yield to precipitation owing to the lack of data to estimate the relationship between crop yield and precipitation. Similar to a previous study⁶, the impact of precipitation was estimated to be low in our model (Supplementary Fig. 6), but the compound effect of temperature and precipitation on crop yield deserves attention^{7,20}. Our yield model is different from previous studies (for example, ref. ⁶) using national crop yield from the Food and Agriculture Organization (FAO) dataset⁴⁰. However, identifying the impact of climate change on national crop yield⁴⁰ can be prevented in some regions in which the impact of historical climate change was not strong enough yet to

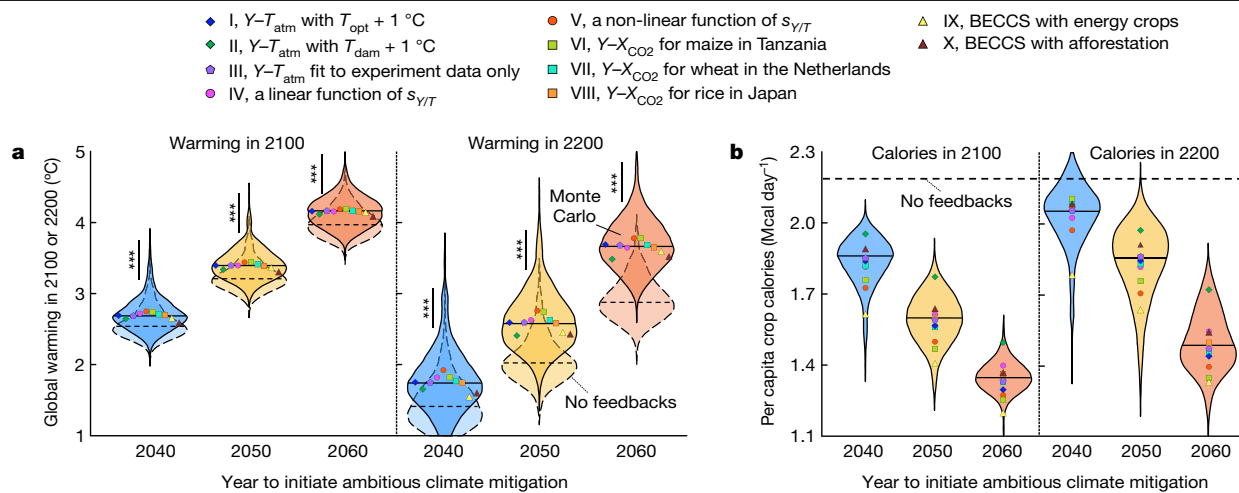


Fig. 3 | Impact of agricultural feedbacks on climate warming and food supply. Violin plots of global warming relative to 1850–1900 (a) and global average per capita calories (b) in 2100 or 2200 when ambitious mitigation is initiated in 2040 (blue), 2050 (yellow) or 2060 (orange), respectively, by deploying large-scale BECCS together with decarbonizing technologies from the SSP2-4.5 scenario² after the year of mitigation onset. The results of scenarios without climate feedbacks on crop yields are obtained by maintaining the simulated capacity of BECCS for current climate (dashed violin plots). The results are estimated from Monte Carlo simulations combining uncertainties in the $Y-T_{atm}$ functions with uncertainties in the Earth system model (Methods). The horizontal line in each violin plot shows

the median estimate. The $Y-T_{atm}$ function is derived from our central case, of which the sensitivity is examined to increasing T_{opt} (I) or T_{dam} by 1 °C (II), using experimental data only to fit the $Y-T_{atm}$ function (III) and fitting the sensitivity⁷ of Y to T_{atm} ($s_{Y/T}$) to a linear (IV) or non-linear (V) function (Supplementary Fig. 3). The $Y-X_{CO2}$ function is derived from our central case or crop models for maize in Tanzania (VI), wheat in the Netherlands (VII) and rice in Japan (VIII)³⁸. We also consider a case with 50% of the cropland expanded from marginal lands for growing energy crops (*Miscanthus*) rather than food crops (IX) and a case with marginal lands converted to forests in afforestation (X). The difference between two neighbouring violin plots is examined (***) for $P < 0.001$.

reduce crop yield substantially⁶. It is important to further improve our crop yield model when data from field-warming experiments become available in a broader range of countries or the regional impacts of climate change on crop yields are more substantial under global warming.

Feedbacks of reduced BECCS capacity to climate change

Our simulations indicated that global warming would reach 2.5 °C (2.3–2.8 °C as the range of 90% uncertainty) in 2050, 2.7 °C (2.4–3.2 °C) in 2100 and 1.7 °C (1.2–2.6 °C) in 2200 (Fig. 3a) if large-scale mitigation alongside BECCS was initiated in 2040 (Methods). Cropland area is expanded to meet the caloric target⁴¹ of 2 million calories per day (Mcal day⁻¹) per capita in 2030 for countries in which the supply is below this threshold and cropland area is maintained for other countries. Owing to the detrimental effects of climate change on crop yields, there is a decline in global average per capita calories from 2.2 Mcal day⁻¹ in 2030 to 1.8 (1.6–2.0) and 2.1 (1.8–2.2) Mcal day⁻¹ in 2100 and 2200, respectively, if the benefits of technology²⁹ were not considered (Fig. 3b). By contrast, global warming is estimated to reach 3.4 and 4.2 °C in 2100, followed by a decrease to 2.6 and 3.7 °C in 2200, if ambitious mitigation is delayed to 2050 and 2060, respectively, because of a longer maintenance of fossil emissions and reduced biomass feedstocks for BECCS. We provided the relationship between the quantity of bioenergy from agricultural residues and the projected level of global warming in 2050, 2100 and 2200 (Supplementary Fig. 7), which could be implemented into IAMs²⁻⁵.

If climate-induced feedbacks on crop yields are not considered by maintaining crop yields and BECCS capacity at their levels simulated with current climatology in 2020, global warming will decrease by 0.3, 0.6 and 0.8 °C in 2200 when ambitious mitigation with BECCS is initiated in 2040, 2050 and 2060, respectively, relative to our central cases (see Supplementary Fig. 8 for the temporal evolutions of global warming and crop calories in all scenarios). Furthermore, global warming will be lower than our central case if 50% of marginal lands are used to grow

dedicated energy crops (such as *Miscanthus*) rather than agricultural crops whose residues are used for BECCS, because energy crops produce more bioenergy than do agricultural crops through the recovery of agricultural residues³⁰. Further, if afforestation is considered together with BECCS by converting marginal lands to forests, global warming will be lower than in the BECCS-only scenarios without afforestation (Fig. 3). Last, if agricultural residues are used to produce liquid bioethanol to replace vehicle oils without carbon capture and storage (CCS) or if the gas-fired power plants were retrofitted for BECCS, the climate benefits of bioenergy would be lower than retrofitting coal-fired power plants for BECCS, owing to the higher CO₂ emissions incurred. If the biomass is used for liquid biofuel production with a high efficiency of energy conversion (47.5%)⁴², then bioenergy at biorefineries generates less climate benefits than BECCS power plants if only 15% of CO₂ released at a high purity during the fermentation process to manufacture bioethanol is subject to CCS⁴³, but generates more benefits than BECCS power plants if 55% of CO₂ in the fermentation process can be captured⁴³. Given different types of bioenergy, the impact of the yield–climate feedback remains robust, which could lead to a failure of meeting the 2 °C goal¹ (Supplementary Fig. 9).

After propagation of uncertainties, the probability of meeting the 2 °C goal¹ by 2200 would be reduced from 47% to 3% after considering agricultural feedbacks when mitigation is initiated in 2050. If mitigation is initiated in 2040, this probability only decreases from 93% to 75% by considering agricultural feedbacks. We examined the sensitivity of our results to the choice of yield–temperature functions fitted to experimental data only, fitting the $Y-T_{atm}$ function to the sensitivity of crop yields to temperature⁷, increasing T_{opt} or T_{dam} by 1 °C when constraining the $Y-T_{atm}$ function and adopting the $Y-X_{CO2}$ relationship for maize in Tanzania, wheat in the Netherlands or rice in Japan from crop models³⁸ (Supplementary Fig. 3). The impact of feedbacks on failure to meet the 2 °C goal¹ owing to delayed mitigation remains robust, but the crop caloric production could be increased or decreased using those alternative yield–climate relationships (Fig. 3). We did not account for all possible factors that could further limit BECCS capacity, such as soil

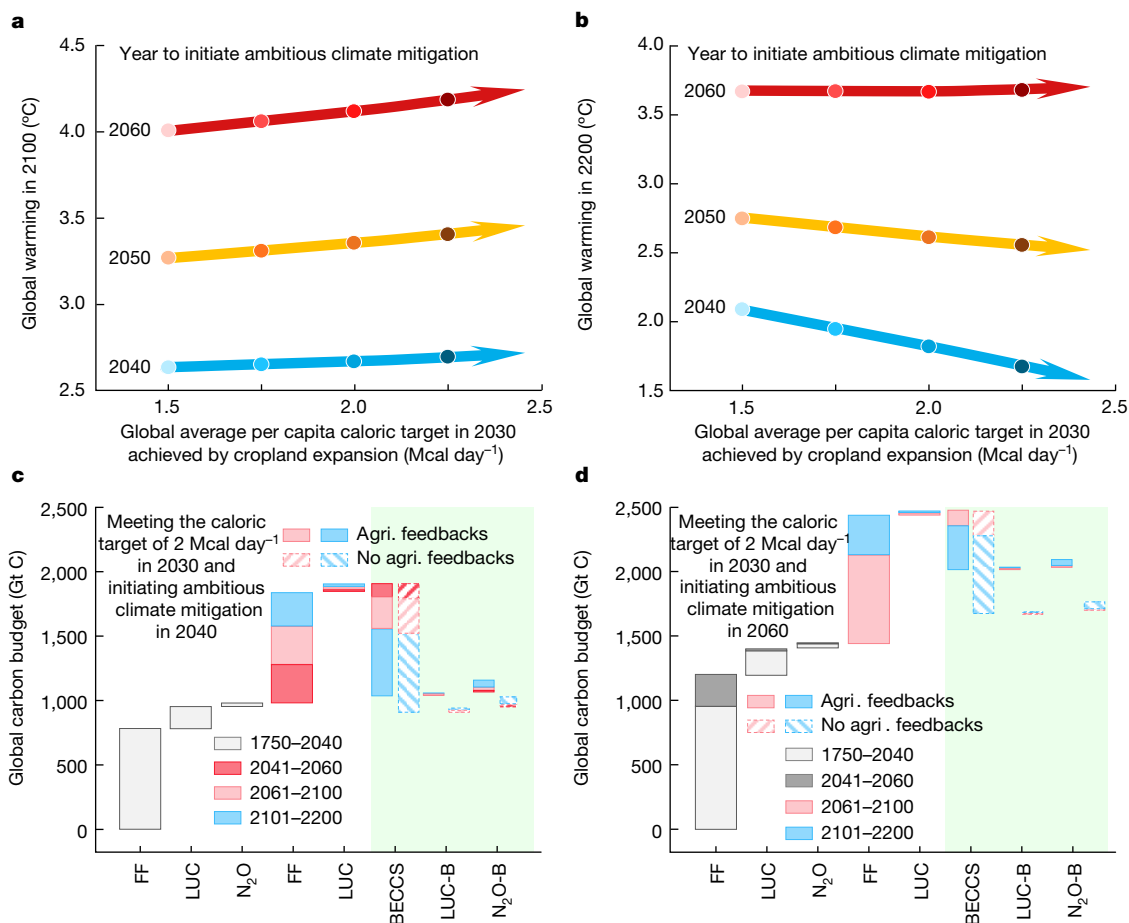


Fig. 4 | The nexus of bioenergy, climate warming and food security. **a,b**, Global warming in 2100 (**a**) and 2200 (**b**) relative to 1850–1900 when cropland area is increased by first converting marginal lands and then forests to cropland to meet the caloric targets of 1.5–2.5 Mcal day⁻¹ in 2030. Climate mitigation is initiated in 2040, 2050 or 2060 by deploying large-scale BECCS with other decarbonizing technologies in the SSP2-4.5 scenario². The higher caloric targets show the impact of larger cropland areas that increases not only BECCS negative emissions but also N₂O emissions and CO₂ emissions owing to LUC.

c,d, Global C budget with (unhatched) or without (hatched) feedbacks of reduced BECCS capacity owing to reduced crop yields when cropland area is expanded to meet the caloric target of 2 Mcal day⁻¹ in 2030 and when global mitigation with large-scale BECCS is initiated in 2040 (**c**) or 2060 (**d**). The cascading bars show a decomposition of the C budget into fossil fuel (FF) emissions, emissions owing to LUC and terrestrial emissions of N₂O, BECCS, LUC emissions owing to BECCS (LUC-B) and N₂O emissions owing to BECCS (N₂O-B) from 1750 to 2200.

degradation¹² or imbalanced nitrogen–phosphorus supplies⁴⁴, so our model may be optimistic and meeting the Paris goals¹ may require even earlier or more ambitious mitigation than we estimated.

Implications for food security

The previous section demonstrated a failure of delayed mitigation to meet the climate goal¹ of 2 °C as climate warming reduces crop yields and BECCS capacity, but the demand on crops for food needs to be considered together with bioenergy production. We assessed whether enlarging cropland area by converting marginal lands and forests to cropland would ameliorate the conflict between food crops and BECCS by considering their impact on the global C cycle through LUC emissions. To do so, we assumed that first marginal lands and then forests are converted to cropland or that N fertilization is increased (see Supplementary Fig. 10 for the spatial distributions of per capita cropland area and N fertilization in 2019) to meet higher caloric targets in 2030. The food supply then depends on the responses of crop yields to climate change (Methods).

Global mitigation by 2050 is needed to match the increasing food demand in the face of decreasing crop yields (Fig. 4). Global warming will be higher in 2100 owing to LUC emissions but lower in 2200 owing to more BECCS negative emissions when mitigation is initiated

earlier than 2050. We decomposed the changes in GHG emissions into its drivers. Total emissions during 2041–2200 to meet a reasonable per capita caloric target⁴¹ of 2 Mcal day⁻¹ would be 28 Gt C from the reduced terrestrial C sink, 10 Gt C from emissions induced by LUC and 92 Gt C from terrestrial emissions of N₂O (converted to equivalent CO₂) (Methods) when mitigation is initiated in 2040 (Supplementary Fig. 11). Converting marginal lands, rather than forests, to cropland will slow warming (see Supplementary Fig. 12 for the difference between these scenarios) but increase the demand of fertilizers⁴⁴. By contrast, if mitigation is delayed to 2060, cropland expansion will accelerate global warming owing to LUC and N₂O emissions, because the effect of cropland expansion to increase BECCS will be overcome by the reduction of BECCS capacity caused by global warming. The effect of intensifying N fertilization alone on slowing global warming is smaller than in the scenarios of increasing the area of cropland (Supplementary Fig. 13) owing to larger terrestrial emissions of N₂O (Supplementary Fig. 11), saturation of N fertilization (Fig. 2d) and potential co-limitations by water and phosphorus⁴⁵.

Impact of agricultural feedbacks on the C budget

The impact of deploying BECCS on allowable fossil emissions depends on the magnitude of agricultural feedbacks under climate change (Fig. 5).

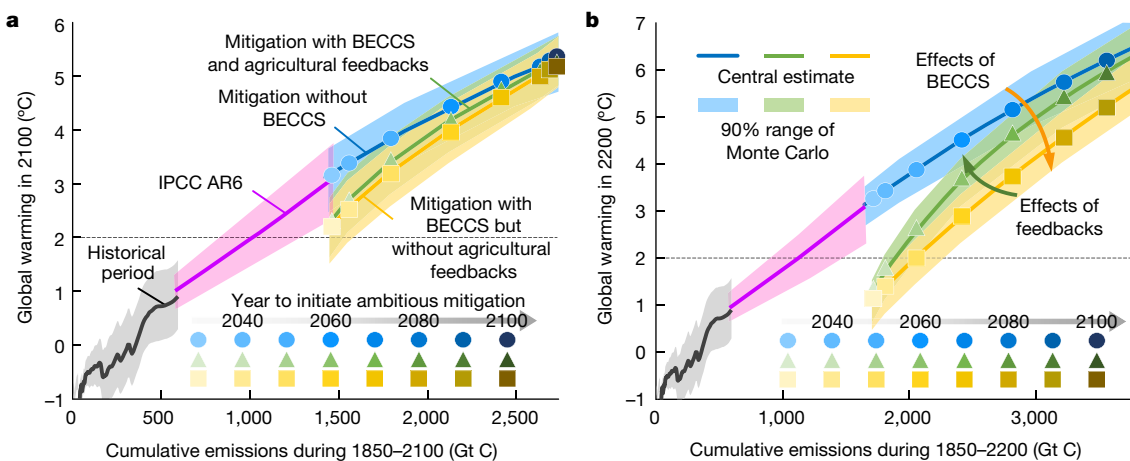


Fig. 5 | Agricultural feedbacks affect the relationship between warming and cumulative CO₂ emissions. Global warming in 2100 (a) or 2200 (b) relative to 1850–1900 is plotted against the cumulative CO₂ emissions by 2100 (a) or 2200 (b), respectively. Historical emissions are identical before 2020, but global climate mitigation starts in different years to deploy large-scale BECCS together with other decarbonizing technologies from the SSP2-4.5 scenario². Global warming in these scenarios without agricultural feedbacks by

To meet the climate goal¹ of 2 °C in 2100 in our central estimate, allowable CO₂ emissions during 1850–2100 increases from 940 to 1,400 Gt C by deploying BECCS without accounting for agricultural feedbacks and to 1,380 Gt C by including them. This negative emission service from BECCS (460 Gt C) agrees with previous model estimates (400–800 Gt C)⁴⁶ but requires that global mitigation actions are initiated by 2030. The impact of agricultural feedbacks on the global C budget is larger in 2200 than in 2100. Allowable CO₂ emissions during 1850–2200 for meeting the target of 2 °C in 2200 increase from 1,120 to 2,040 Gt C by implementing large-scale BECCS when excluding agricultural feedbacks, but only to 1,890 Gt C with them. The effects of agricultural feedbacks in reducing allowable CO₂ emissions will increase as the mitigation is delayed owing to increasing feedbacks to climate warming. For example, agricultural feedbacks would reduce allowable CO₂ emissions by 150 and 270 Gt C to meet the targets of 2 and 3 °C in 2200, respectively. These reductions suggest that the ability to mitigate climate change by BECCS will decrease as a result of delayed mitigation actions.

Regional food gap under climate change

Mitigating climate change requires global early actions through large-scale BECCS implementation², but the impact of climate warming on crop yields varies among regions. On the basis of the yield–climate relationships, warming increases yields of wheat and maize over high-latitude regions with an average growing-season temperature lower than 10 and 19 °C, covering 4% and 30% of the global cropland area, respectively (Supplementary Fig. 14). We define an index of food gap as one minus the ratio of per capita calories to a minimum under-nutrition level of 1.5 Mcal day⁻¹, in which a higher positive food gap indicates a larger shortage of food crops. The effect of a delay from 2040 to 2060 of ambitious climate mitigation by deploying large-scale BECCS together with decarbonizing technologies in the SSP2-4.5 scenario² would be that the food gap in 2100 will increase to >50% in India, Africa and the Middle East without food trade (Fig. 6). Many developing countries are located at lower latitudes and exposed to higher temperatures. Owing to a delay of climate mitigation from 2040 to 2060, the number of developing countries in which the food gap is positive will increase from 81 to 90 in 2100. By contrast, the food gap in 2100 remains negative in developed countries if ambitious mitigation is delayed from 2040 to 2060.

maintaining the capacity of BECCS (orange line) is compared with the result with them (green line). The relationship between global warming and cumulative CO₂ emissions in IPCC AR6 (ref. ²) is indicated by the purple lines. The shaded area indicates the range of 90% uncertainty in Monte Carlo simulations varying climate parameters and yield–climate relationships (Methods).

The gap of food supply in low-latitude developing countries may be alleviated by international trade of crops from temperate and northern countries to Central America, Africa and the Middle East. Export of food crops (such as wheat, rice and maize) from North America (417 Mt year⁻¹), Europe (385 Mt year⁻¹) and China (422 Mt year⁻¹) to the remaining regions of the world is required to reduce the fraction of people with a positive food gap in 2100 from 65% to 30% when mitigation starts in 2060 (Supplementary Fig. 15). The projected export of crops, however, would be 3, 2 and 80 times larger than the current levels⁴⁰ in 2019 for these three regions, respectively, indicating a large and probably implausible extent of increasing trade. Early climate mitigation¹⁰ or population migration⁴⁷ may be the choice we have to make if the necessary food trade fails to occur.

Implications

Our results indicate that the negative impacts of climate change can reduce crop yields and, thus, the BECCS capacity, leading to exceeding the 2 °C Paris goal¹ and threatening food security. This process is absent in the future scenarios from current IAMs relying on large-scale deployment of BECCS during the second half of this century^{2–5,48,49}. The capacity of BECCS could rapidly decrease after reaching a threshold of climate warming. This would be the consequence of reduced biomass feedstocks in response to accelerated global warming owing to a 20-year delay in mitigation from 2040 to 2060. The climate warming threshold, modelled here to occur in around 2050 when global warming exceeds 2.5 °C, is lower than many known ‘tipping points’ in the climate system that would lead to failure of the Paris goals¹, such as triggering the melting of the Greenland ice sheet or the collapse of the Atlantic thermohaline circulation⁵⁰. Exceeding the warming threshold above will jeopardize food security in most developing countries, with a potential impact on developed countries. Accounting for these feedbacks improves our understanding of the food–climate–energy nexus and reinforces the importance of early and ambitious mitigation¹⁰ to meet the Paris goals².

Delayed mitigation of CO₂ emissions inevitably requires a larger effort by deploying BECCS negative emissions, lasting for a longer time to offset the positive fossil emissions². Food crises owing to an unprecedented climate change may also lead to a shift of the growing season⁷ and to population migration⁴⁷. As a caveat, our study may

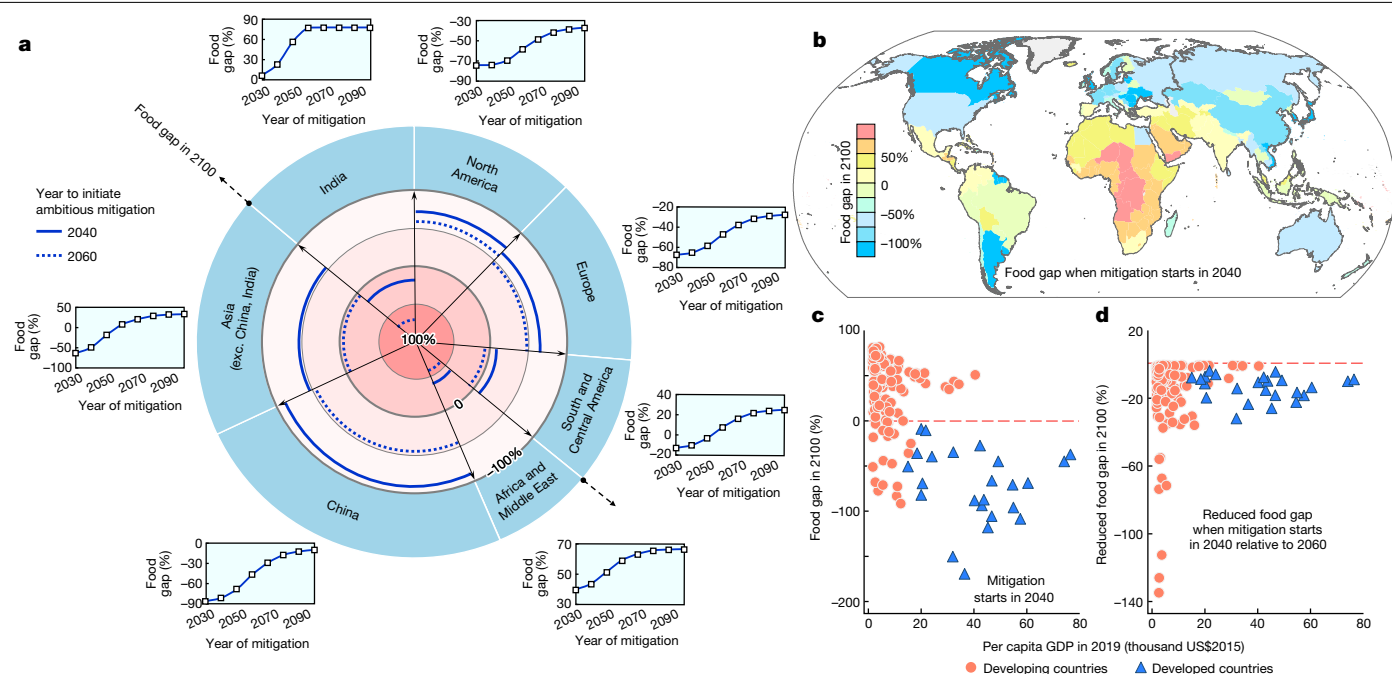


Fig. 6 | Contribution of climate mitigation to reduce the regional food gap. **a**, Regional food gap, defined as one minus the ratio of per capita calories to a minimum undernutrition level of $1.5 \text{ Mcal day}^{-1}$, in 2100. A higher food gap indicates a larger shortage of food crops. Ambitious mitigation is initiated in 2040 (solid line) or 2060 (dotted line) by deploying large-scale BECCS together with other decarbonizing technologies from the SSP2-4.5 scenario². The area of the pie chart is proportional to current crop caloric production in 2019.

overestimate future food shortages because we did not consider all potential benefits of advancing technologies and optimizing managements⁵¹. As half of the N added to cropland is at present lost to the environment³², and in many countries N fertilization is already very high, food shortage could be alleviated by increasing the N use efficiency with better phosphorus and potassium fertilization so as to reach an adequate balance among these three fertilizers⁴⁴. For example, if the N use efficiency was increased following a recent projection²⁹ to increase N uptake by region and reduce N_2O emissions⁵³ for global croplands, per capita calories are projected to increase by 10% with a reduction of global warming by $0.2 \text{ }^\circ\text{C}$ in 2200 when mitigation is initiated in 2050 (Supplementary Fig. 16). We also projected an increase in per capita calories by 11% and a reduction of global warming by $0.3 \text{ }^\circ\text{C}$ in 2200 if we bring forward or delay the growing season for each country to optimize the crop yield under future, warmer climatology. Assuming that humanity can moderate the increase of N fertilizers use and achieve a better N use efficiency (by crops taking up more N and getting more benefits from the N applied) by equilibrating fertilization⁴⁴, improving water use and developing new crop varieties⁵¹, technologies will further alleviate the shortage of food and increase the capacity of BECCS. Even so, if ambitious mitigation of CO_2 emissions with a heavy reliance on BECCS is delayed, the impact of yield-climate feedbacks could still lead to a failure of meeting the $2 \text{ }^\circ\text{C}$ goal in the Paris Agreement¹ by considering the interactions between crop yield and climate warming (Supplementary Fig. 16). Accounting for these feedbacks substantially undermines the feasibility of high allowable fossil-fuel emissions under overshoot scenarios¹³ of delayed mitigation relying heavily on BECCS after 2050 to limit global warming below $2 \text{ }^\circ\text{C}$ (refs. 2-5,48,49).

Our findings support the concerns of overshooting temperature targets by relying solely on BECCS and the assumption that BECCS production would remain insensitive to climate change³. They also indicate that irreversible climate change and serious food crises should be best

avoided by accelerating supply-side decarbonization⁵⁴ if the reduced capacity of BECCS cannot be compensated by other negative-emission technologies. Although biophysical and technological barriers of BECCS have been widely recognized^{3,11,12,14,48,49}, our results underscore an unrecognized drawback of BECCS owing to agricultural feedbacks that limit BECCS capacity to mitigate climate change in cases of delayed mitigation. If the climate benefits of BECCS were to be attained, this technology should be deployed as early as possible, otherwise the decreasing biomass feedstocks will reduce the BECCS efficacy and lead to failure of meeting the Paris goal of $2 \text{ }^\circ\text{C}$ (ref. 1), even by 2200. If the large-scale BECCS project cannot be put into place in the near term, these feedbacks will inevitably reduce the allowable emissions more than previously thought: demand-side decarbonization and other negative-emission technologies should undergo a more rapid deployment for human society to stay within the safe boundaries in regards to climate change.

Online content

Any methods, additional references, Nature Research reporting summaries, source data, extended data, supplementary information, acknowledgements, peer review information; details of author contributions and competing interests; and statements of data and code availability are available at <https://doi.org/10.1038/s41586-022-05055-8>.

1. United Nations Framework Convention on Climate Change (UNFCCC). *Paris Agreement - Status of Ratification* <https://unfccc.int/process/the-paris-agreement/status-of-ratification> (2021).
2. Intergovernmental Panel on Climate Change (IPCC). *Climate Change 2021: The Physical Science Basis. Contribution of Working Group I to the Sixth Assessment Report of the Intergovernmental Panel on Climate Change* (eds Masson-Delmotte, V. et al.) <https://www.ipcc.ch/assessment-report/ar6/> (Cambridge Univ. Press, 2021).
3. Fuss, S. et al. Betting on negative emissions. *Nat. Clim. Change* **4**, 850–853 (2014).
4. Rogelj, J. et al. Scenarios towards limiting global mean temperature increase below $1.5 \text{ }^\circ\text{C}$. *Nat. Clim. Change* **8**, 325–332 (2018).

5. Muratori, M. et al. EMF-33 insights on bioenergy with carbon capture and storage (BECCS). *Clim. Change* **163**, 1621–1637 (2020).
6. Lobell, D. B., Schlenker, W. & Costa-Roberts, J. Climate trends and global crop production since 1980. *Science* **333**, 616–620 (2011).
7. Zhao, C. et al. Field warming experiments shed light on the wheat yield response to temperature in China. *Nat. Commun.* **7**, 13530 (2016).
8. Su, Y., Gabrielle, B. & Makowski, D. The impact of climate change on the productivity of conservation agriculture. *Nat. Clim. Change* **11**, 628–633 (2021).
9. Gasser, T. et al. The compact Earth system model OSCAR v2.2: description and first results. *Geosci. Model Dev.* **10**, 271–319 (2017).
10. Meinshausen, M. et al. Realization of Paris Agreement pledges may limit warming just below 2 °C. *Nature* **604**, 304–309 (2022).
11. Jones, M. B. & Albanito, F. Can biomass supply meet the demands of bioenergy with carbon capture and storage (BECCS)? *Glob. Change Biol.* **26**, 5358–5364 (2020).
12. Creutzig, F. et al. Considering sustainability thresholds for BECCS in IPCC and biodiversity assessments. *Glob. Change Biol. Bioenergy* **13**, 510–515 (2021).
13. Johansson, D. J. A. The question of overshoot. *Nat. Clim. Change* **11**, 1021–1022 (2021).
14. Hasegawa, T. et al. Land-based implications of early climate actions without global net-negative emissions. *Nat. Sustain.* **4**, 1052–1059 (2021).
15. Lenton, T. M. et al. Climate tipping points — too risky to bet against. *Nature* **575**, 592–595 (2019).
16. van Vuuren, D. P. et al. Alternative pathways to the 1.5 °C target reduce the need for negative emission technologies. *Nat. Clim. Change* **8**, 391–397 (2018).
17. Rickels, W., Merk, C., Reith, F., Keller, D. P. & Oeschlies, A. (Mis)conceptions about modeling of negative emissions technologies. *Environ. Res. Lett.* **14**, 104004 (2019).
18. Lu, X. et al. Gasification of coal and biomass as a net carbon-negative power source for environment-friendly electricity generation in China. *Proc. Natl Acad. Sci. USA* **116**, 8206–8213 (2019).
19. Xing, X. et al. Spatially explicit analysis identifies significant potential for bioenergy with carbon capture and storage in China. *Nat. Commun.* **12**, 3159 (2021).
20. Schyns, J. F. et al. Limits to the world's green water resources for food, feed, fiber, timber, and bioenergy. *Proc. Natl Acad. Sci. USA* **116**, 4893–4898 (2019).
21. Hanssen, S. V. et al. Biomass residues as twenty-first century bioenergy feedstock—a comparison of eight integrated assessment models. *Clim. Change* **163**, 1569–1586 (2020).
22. Kukul, M. S. & Irmak, S. Climate-driven crop yield and yield variability and climate change impacts on the U.S. Great Plains agricultural production. *Sci Rep.* **8**, 3450 (2018).
23. Yoshida, R. et al. Adaptation of rice to climate change through a cultivar-based simulation: a possible cultivar shift in eastern Japan. *Clim. Res.* **64**, 275–290 (2015).
24. Spinoni, J. et al. How will the progressive global increase of arid areas affect population and land-use in the 21st century? *Glob. Planet. Change* **205**, 103597 (2021).
25. Lade, S. J. et al. Human impacts on planetary boundaries amplified by Earth system interactions. *Nat. Sustain.* **3**, 119–128 (2020).
26. Milkoreit, M. et al. Defining tipping points for social-ecological systems scholarship—an interdisciplinary literature review. *Environ. Res. Lett.* **13**, 033005 (2018).
27. Hausfather, Z. & Peters, G. Emissions – the ‘business as usual’ story is misleading. *Nature* **577**, 618–620 (2020).
28. Potapov, P. et al. Global maps of cropland extent and change show accelerated cropland expansion in the twenty-first century. *Nat. Food* **3**, 19–28 (2022).
29. Zhang, X. et al. Managing nitrogen for sustainable development. *Nature* **528**, 51–59 (2015).
30. Fajardy, M. & Mac Dowell, N. Can BECCS deliver sustainable and resource efficient negative emissions? *Energy Environ. Sci.* **10**, 1389–1426 (2017).
31. Friedlingstein, P. et al. Global carbon budget 2020. *Earth Syst. Sci. Data* **12**, 3269–3340 (2020).
32. Moore, C. E. et al. The effect of increasing temperature on crop photosynthesis: from enzymes to ecosystems. *J. Exp. Bot.* **72**, 2822–2844 (2021).
33. Asseng, S. et al. Rising temperatures reduce global wheat production. *Nat. Clim. Change* **5**, 143–147 (2015).
34. Asseng, S. et al. The upper temperature thresholds of life. *Lancet Planet. Health* **5**, e378–e385 (2021).
35. Ainsworth, E. A. & Long, S. P. What have we learned from 15 years of free-air CO₂ enrichment (FACE)? A meta-analytic review of the responses of photosynthesis, canopy properties and plant production to rising CO₂. *New Phytol.* **165**, 351–372 (2005).
36. Wang, S. et al. Recent global decline of CO₂ fertilization effects on vegetation photosynthesis. *Science* **370**, 1295–1300 (2020).
37. Broberg, M. C. et al. Effects of elevated CO₂ on wheat yield: non-linear response and relation to site productivity. *Agronomy* **9**, 243 (2019).
38. Makowski, D. et al. A statistical analysis of three ensembles of crop model responses to temperature and CO₂ concentration. *Agric. For. Meteorol.* **7**, 483–493 (2015).
39. Wang, D. et al. Excessive nitrogen application decreases grain yield and increases nitrogen loss in a wheat–soil system. *Acta Agric. Scand. B Soil Plant Sci.* **61**, 681–692 (2011).
40. Food and Agriculture Organization of the United Nations (FAO). *FAOSTAT* <https://www.fao.org/faostat/en/#data> (2021).
41. Food and Agriculture Organization of the United Nations (FAO). *Human Energy Requirements* <https://www.fao.org/3/y5686e/y5686e.pdf> (2001).
42. Muratori, M. et al. Carbon capture and storage across fuels and sectors in energy system transformation pathways. *Int. J. Greenh. Gas Control.* **57**, 34–41 (2017).
43. Fajardy, M., Koeberle, A., MacDowell, N. & Fantuzzi, A. *BECCS Deployment: A Reality Check. Grantham Institute Briefing paper No 28* <https://www.imperial.ac.uk/media/imperial-college/grantham-institute/public/publications/briefing-papers/BECCS-deployment---a-reality-check.pdf> (2019).
44. Peñuelas, J. & Sardans, J. The global nitrogen-phosphorus imbalance. *Science* **375**, 266–267 (2022).
45. Ye, Y. et al. Carbon, nitrogen and phosphorus accumulation and partitioning, and C:N:P stoichiometry in late-season rice under different water and nitrogen managements. *PLoS One* **9**, e101776 (2014).
46. Gasser, T., Guivarch, C., Tachiiri, K., Jones, C. D. & Ciais, P. Negative emissions physically needed to keep global warming below 2 °C. *Nat. Commun.* **6**, 7958 (2015).
47. Boas, I. et al. Climate migration myths. *Nat. Clim. Change* **9**, 901–903 (2019).
48. Riahi, K. et al. Cost and attainability of meeting stringent climate targets without overshoot. *Nat. Clim. Change* **11**, 1063–1069 (2021).
49. Drouet, L. et al. Net zero-emission pathways reduce the physical and economic risks of climate change. *Nat. Clim. Change* **11**, 1070–1076 (2021).
50. Lenton, T. M. et al. Tipping elements in the Earth's climate system. *Proc. Natl Acad. Sci. USA* **105**, 1786–1793 (2008).
51. van Zeist, W. J. et al. Are scenario projections overly optimistic about future yield progress? *Glob. Environ. Change* **64**, 102120 (2020).
52. Lassaletta, L., Billen, G., Grizzetti, B., Anglade, J. & Garnier, J. 50 year trends in nitrogen use efficiency of world cropping systems: the relationship between yield and nitrogen input to cropland. *Environ. Res. Lett.* **9**, 105011 (2014).
53. Thilakarathna, S. K. et al. Nitrous oxide emissions and nitrogen use efficiency in wheat: nitrogen fertilization timing and formulation, soil nitrogen, and weather effects. *Soil Sci. Soc. Am. J.* **84**, 1910–1927 (2020).
54. Wang, R., Saunders, H., Moreno-Cruz, J. & Caldeira, K. Induced energy-saving efficiency improvements amplify effectiveness of climate change mitigation. *Joule* **3**, 2103–2119 (2019).

Publisher's note Springer Nature remains neutral with regard to jurisdictional claims in published maps and institutional affiliations.

Springer Nature or its licensor holds exclusive rights to this article under a publishing agreement with the author(s) or other rightsholder(s); author self-archiving of the accepted manuscript version of this article is solely governed by the terms of such publishing agreement and applicable law.

© The Author(s), under exclusive licence to Springer Nature Limited 2022

Methods

Earth system model

We used a compact Earth system model, OSCAR 2.2, to simulate climate change during historical and future periods driven by emissions of GHGs from human activities. Detailed descriptions of this model are provided by Li et al.⁵⁵, Gasser et al.⁹⁵⁶ and Fu et al.⁵⁷. The interactions between climate change and the C cycle in terrestrial systems were calibrated using the CMIP models³¹. In this study, we implemented the yield–climate relationships into the OSCAR model to simulate the interactions between climate change and agricultural development in assumed scenarios of cropland expansion and intensified N fertilization and to evaluate the impact of agriculture feedbacks on climate change under temperature overshoots¹³. Total anthropogenic CO₂ emissions from fossil-fuel combustion and cement production before 2010 were obtained from the CDIAC dataset⁵⁸, anthropogenic emissions of methane (CH₄), N₂O, nitrogen oxides (NO_x), carbon monoxide (CO), volatile organic compounds (VOCs), sulfur dioxide (SO₂), ammonia (NH₃), 11 hydrofluorocarbons, eight perfluorocarbons and 16 ozone-depleting substances were obtained from the EDGAR inventory⁵⁹, anthropogenic and natural emissions of organic carbon (OC) and black carbon (BC) were obtained from the ACCMIP inventory⁶⁰ and the GFED v3.1 inventory⁶¹ and emissions of CO₂ and non-CO₂ GHGs owing to LUC were obtained from the LUH1.1 dataset⁶². Forcing data after 2010 were compiled from the SSP5-8.5 and SSP2-4.5 (excluding the contribution of negative emissions)², including data for anthropogenic emissions of CO₂, CH₄, N₂O, NO_x, CO, VOCs, BC, OC, SO₂, NH₃, 11 hydrofluorocarbons, eight perfluorocarbons and 16 ozone-depleting substances.

The model was run with active interactions and feedbacks between various Earth elements⁶³, in which the elements interacting with each other in the Earth system represented the responses of the climatic system to anthropogenic perturbations such as GHG emissions from industrial processes, cropland expansion, LUC and intensified N fertilization. Changes in global C budgets and GHG emissions were modelled using the terrestrial C sink, LUC emissions and the terrestrial emissions of N₂O. This model configuration allowed us to simulate the feedbacks of both climate change to agricultural activities and of agricultural yields to climate change. Calculations of the changes in atmospheric concentrations of CO₂, tropospheric and stratospheric chemistry, surface albedo, terrestrial C sinks, LUC emissions, air–sea gas exchanges and the regional responses of atmospheric temperature and precipitation to the climatic forcers in the OSCAR model were identical to those in previous studies^{9,55–57}, with a limit to the simulated concentrations of N₂O and CH₄ (420 ppb for N₂O and 2,200 ppb for CH₄).

Net primary production in cropland

The net primary production for cropland (NPP, g C year⁻¹) in year t was represented by a function of crop yield (Y_{it} , g biomass ha⁻¹ year⁻¹) and cropland area (A_{it} , ha):

$$NPP_t = \sum_{i=1}^8 \frac{A_{it} Y_{it} \mu_i f_i}{v_i I_i} \quad (1)$$

in which i is the crop, v_i is the fraction of shoots in the biomass, μ_i is the fraction of dry biomass, f_i is the fraction of C in the dry biomass and I_i is a harvest index, defined as the ratio of the mass of the harvested yield to above-ground biomass. We divided all crops into eight categories: cereals, roots and tubers, beans, oil crops, fibre crops, sugar crops, primary fruits and primary vegetables. The values of the parameters μ_i , v_i , f_i and I_i for these categories are listed in Supplementary Table 4.

In our model, the crop yield (Y_{it}) in year t was predicted as:

$$Y_{it} = Y_{i0} \frac{F^C(C_t) F^T(T_t) F^Z(Z_t) F^P(P_t)}{F^C(C_0) F^T(T_0) F^Z(Z_0) F^P(P_0)} \quad (2)$$

in which Y_{i0} (g biomass ha⁻¹ year⁻¹) is the yield in 2019 and C_t , T_t , Z_t and P_t denote atmospheric CO₂ concentration, average temperature during the growing season, cropland intensity of N fertilization and precipitation in a future year t , respectively. F^C , F^T , F^Z and F^P were estimated from the relationships between observed crop yields and atmospheric CO₂ concentration (C_t , ppm), atmospheric mean growing-season temperature (T_t , °C), intensity of N fertilization (Z_t , kg N ha⁻¹) and precipitation (P_t , mm year⁻¹), respectively:

$$F^C(C_t) = \beta^C C_t^2 + \gamma^C C_t + \alpha^C \quad (3)$$

$$F^T(T_t) = \beta^T T_t^2 + \gamma^T T_t + \alpha^T \quad (4)$$

$$F^Z(Z_t) = \gamma^Z \ln(Z_t) + \alpha^Z \quad (5)$$

$$F^P(P_t) = \exp(\gamma^P \Delta P_t) \quad (6)$$

in which the coefficients α^C , β^C , γ^C , α^T , β^T , γ^T , α^Z and γ^Z were determined by fitting these functions to data (Supplementary Data Set 1). We compiled the yield data for maize and wheat from both field-warming experiments and local process-based or statistical models (Supplementary Table 2). After excluding data with a narrow range of growing-season temperature or without controlling the impact of confounding variables, our dataset covers 13 countries globally distributed in Africa, East Asia, South Asia, West Asia, North America and South and Central America, in which the average growing-season temperature ranges from 12 to 34 °C. As the environments for these experiments are different, it is necessary to normalize the variance of the yields between different studies. This is done by dividing the yields by the average yields measured around 25 °C using 10% of data. To constrain the yield–temperature functions, we compiled the optimal growing temperature (T_{opt}) for maize and wheat growing in different countries or regions (Supplementary Table 3). We fit the yield–temperature functions to the local data in the USA, India, Sudan, Mexico, China, Pakistan and Africa using the local T_{opt} if applicable or using the average T_{opt} (Supplementary Fig. 3), and we fit the global yield–temperature functions to all data applying the average T_{opt} (Fig. 2).

In our Earth system model, we used the yield–temperature functions fit to the local data to predict the future crop yields in these countries if applicable and used the yield–temperature functions fit to the global data in the remaining regions of the world. We did not find long-term data for other crops and assumed that the yield–temperature function for other crops is similar to that of wheat. We estimated uncertainties in the fitted functions (Fig. 2 and Supplementary Fig. 3), which were considered in our Monte Carlo Earth system model simulations to estimate the climate impact of deploying BECCS. We performed more experiments to examine the sensitivity of the yield–temperature relationship to using only experimental data, increasing the optimal growing temperature (T_{opt}) or the dampening temperature (T_{dam}) by 1 °C and using a linear or non-linear function to fit the sensitivity of wheat yield to temperature change⁷ (Supplementary Fig. 3), which are considered to examine the sensitivity of the climate benefits of BECCS to these factors (Fig. 3).

The fitted parameters α^T , β^T and γ^T using all data and the fitted α^C , β^C , γ^C , α^Z and γ^Z are listed by region in Supplementary Table 5. Different from the parameters in the response of crop yields to changes in temperature, atmospheric CO₂ and intensity of N fertilization, the parameter γ^P in the response of crop yield to change in precipitation was determined by a previous study⁹. In that study, crop yield was simulated using seven Earth system models^{31,63} in a case using a fully coupled configuration with an increase of atmospheric CO₂ of +1% year⁻¹, in a case using the fixed climate and in a case using the fixed carbon cycle, respectively. For each region, an exponential function was used to fit the simulated crop yields based on the decadal moving averages of the relevant variables

Article

in the seven models, in which the best fit returned the parameter γ^p in the response of crop yield to precipitation in each region. As a caveat, γ^p was not determined as other parameters owing to the lack of field experiments measuring the response of crop yield to precipitation change, but, similar to a previous study⁶, the impact of precipitation on crop yields in the future was estimated at a lower magnitude than temperature, atmospheric CO₂ and intensity of N fertilization in our model (Supplementary Fig. 6).

For future scenarios, we predicted the yields of eight crops (cereals, roots and tubers, beans, oil crops, fibre crops, sugar crops, primary fruits and primary vegetables) (Y_t) based on the yield of each crop for the year 2019 from the FAO dataset⁴⁰ and the changes in N fertilization, CO₂ concentrations and the average growing-season temperature and precipitation over croplands from 2019 to a future year during 2020–2200 by country. The crop yields (Y_{2019}), N fertilization (Z_{2019}), CO₂ concentration (C_{2019}) and the average growing-season temperature and precipitation over cropland (T_{2019} and P_{2019} , respectively) for 167 countries in 2019 are listed in Supplementary Data Set 2. For dedicated energy crops, the average yield (8.5 t ha⁻¹) in 2020 was derived from a previous study⁶⁴ as a conservative estimate. The yield of dedicated energy crops under climate change is predicted by equations (2)–(6) using the functions of atmospheric CO₂ concentration, atmospheric surface temperature, N fertilization and precipitation, as for wheat crop.

Terrestrial C sink

The terrestrial C sink, which is one of the drivers of changes in atmospheric CO₂ concentration, responds to changes in atmospheric CO₂ concentration and other environmental changes. The OSCAR model⁹ divided global land into five categories: bare soil, forest, grassland and shrubland, cropland and pasture. The change in the terrestrial C sink ($\Delta E_{\downarrow land}$, Gt C year⁻¹) for each biome relative to the pre-industrial period (1850–1900) was estimated as:

$$\Delta E_{\downarrow land} = (\Delta e_t^{fire} + \Delta r h_t^{litter} + \Delta r h_t^{soil} - \Delta NPP_t) (A_0 + \Delta A_t) \quad (7)$$

in which A_0 is the pre-industrial area for this biome, ΔA_t is the change in area relative to the pre-industrial period, Δe_t^{fire} is the change in the flux of C from biomass burnt in wildfires, $\Delta r h_t^{litter}$ is the change in the flux of C from biomass to the atmosphere when C in litter is oxidized by heterotrophic respiration, $\Delta r h_t^{soil}$ is the change in the flux of C from soil to the atmosphere when soil C is oxidized by heterotrophic respiration and ΔNPP_t is the intensive change in net primary production. Δe_t^{fire} was calculated as a function of the fire intensity and the amount of living biomass, in which the fire intensity was represented as a function of surface air temperature, precipitation and atmospheric CO₂ concentration⁹. $\Delta r h_t^{litter}$ was calculated as a function of the litter C concentration, annual mean atmospheric temperature and precipitation⁵⁷. $\Delta r h_t^{soil}$ was calculated as a function of the soil C concentration, annual mean atmospheric temperature and precipitation⁹. ΔNPP_t was calculated for cropland using equation (1) and for other biomes as a function of atmospheric CO₂ concentration, annual mean atmospheric temperature and precipitation⁹.

LUC emissions of CO₂

The conversion of marginal lands first and then forests to cropland to meet the increasing food targets leads to further LUC emissions of CO₂ by affecting the stock of C in living biomass, litter and soil C pools and harvested wood products. LUC emissions (ΔE_{LUC}) depend on the changes in C stocks in different pools:

$$\Delta E_{LUC} = -\frac{d}{dt} \left(\Delta C_{veg} + \Delta C_{litter} + \Delta C_{soil} + \sum_p \Delta C_{hwp}^p \right) \quad (8)$$

in which p is the use of a wood product (1 for fuel wood, 2 for pulp-based products and 3 for hardwood-based products) and ΔC_{veg} , ΔC_{litter} , ΔC_{soil}

and ΔC_{hwp} indicate the stocks of C in living biomass, litter, soil and harvested wood products, respectively. ΔC_{veg} , ΔC_{litter} , ΔC_{soil} and ΔC_{hwp} were calculated on the basis of the changes in the area from one biome to another biome and on the C concentration in each pool. The C concentration in each pool was simulated using the dynamic scheme that is calibrated by the flux of C in the CMIP5 model⁶³. The total LUC emissions from 1800 to 2020 are estimated at 137 Gt C, which is in the range of the estimates since 1800 (100–180 Gt) by Erb et al.⁶⁵.

N₂O emissions

N₂O was treated as a well-mixed GHG in the OSCAR model. Anthropogenic sources of N₂O include direct and indirect emissions from agriculture, energy production, industry, waste and wildfires^{59,66,67}. Natural sources of N₂O include emissions from tropical soils⁶⁸ and emissions from the application of N fertilizers⁶⁹. N₂O in the atmosphere is mainly removed by stratospheric photolysis, the rate of which is a function of the stratospheric N₂O concentration owing to the autocatalytic feedback of N₂O by reducing the concentration of stratospheric ozone⁷⁰. For the future simulations, we modelled the agricultural practice of N fertilization with the average length of growing season (153 days)⁶⁹. N₂O emissions were converted to equivalent CO₂ emissions using a constant ratio of 81.3 g C to 1 g N₂O (ref. ⁶⁹). For the future scenarios, N₂O emissions converted to equivalent CO₂ emissions ($\Delta E_{N2O-fertilizer}$, t C year⁻¹) owing to agricultural N fertilization in cropland were represented by an exponential function⁶⁹:

$$\Delta E_{N2O-fertilizer} = 4.93 \cdot D \cdot A \cdot \sigma_{N2O} \cdot \exp(0.0134 \cdot Z) \quad (9)$$

in which Z is the intensity of N fertilization in the cropland (kg ha⁻¹), D is the duration of N fertilization, A is the area of cropland and σ_{N2O} is the coefficient for converting N₂O emissions to equivalent CO₂ emissions.

Average growing-season temperature in cropland

We used the OSCAR model to simulate the average atmospheric temperature (T_{jt}) in cropland in region j in year t during the growing season based on the pre-industrial temperature for cropland in region j during the growing season (T_{j0}) and degree of global warming relative to the pre-industrial period (1850–1900) (ΔT_{jt}):

$$T_{jt} = T_{j0} + \omega_j \Delta T_t \quad (10)$$

in which j is the region (1 for North America, 2 for South and Central America, 3 for Europe, 4 for the Middle East and northern Africa, 5 for tropical Africa, 6 for the former Soviet Union, 7 for China, 8 for southern and south-eastern Asia and 9 for the developed Pacific region) and ω_j is the ratio of regional to global warming, calibrated for each region from an ensemble of CMIP models³¹. Atmospheric surface temperature differs between cropland and other land types and between the growing and non-growing seasons in a region, so we assumed that the change in atmospheric growing-season temperature was homogeneous in a region. We estimated the average growing-season temperature by country based on global crop calendar data⁷¹ (Supplementary Data Set 3).

The degree of global warming (ΔT_t) was simulated as a function of anthropogenic radiative forcing (ΔRF) of GHGs, ozone precursors, aerosols and aerosol precursors and the natural forcings caused by various anthropogenic activities:

$$\tau \frac{d}{dt} \Delta T_t = \lambda \Delta RF - \Delta T_t - \theta (\Delta T_t - \Delta D_t) \quad (11)$$

in which τ is the temporal inertia of global mean atmospheric temperature, λ is the equilibrium climate sensitivity, θ is the coefficient determining exchange of energy between the Earth surface and deep oceans and ΔD is the change in temperature of deep oceans. These parameters are identical to those determined by previous studies^{55–57}.

In the OSCAR model, we calibrated the pre-industrial surface air temperature in the growing season over cropland (T_{j0}) in country j using the observed average temperature in the growing season in cropland for 2016–2019 ($T_{j,2016-2019}$) in country j and the simulated change in atmospheric surface temperature in this country in 2019 relative to the average of 1850–1900 ($\Delta T_{j,1900-2019}$). Atmospheric temperature in the growing season in cropland for 2016–2019 by country ($T_{j,2016-2019}$) was estimated from the global gridded daily temperature reanalysis dataset of the Global Forecast System released by the National Centers for Environmental Prediction⁷².

Global data of crop yields, cropland area and N fertilization

We compiled the yields of crops by country for 1961–2019 from the FAO global agricultural dataset⁴⁰. We simulated the national crop yields for 2020–2200 using equations (2)–(6) based on the simulated atmospheric CO₂ concentration, the simulated average growing-season temperature, the simulated precipitation and the targeted intensity of N fertilization. We compiled the national areas of cropland growing cereals, roots and tubers, beans, oil crops, fibre crops, sugar crops, primary fruits and primary vegetables for 1961–2019 from the FAO global agricultural dataset of cropland area⁴⁰. The area of marginal lands is derived from a previous study⁷³. We applied the per capita cropland area in 2020 to the period from 2020 to 2200 as a constant in the scenario without cropland expansion. In the scenarios of cropland expansion, we increased the per capita cropland area in 2020 to a specific area (0.16, 0.17, ..., 0.24 ha) to meet the caloric targets of 1.5–2.5 Mcal day⁻¹ in 2030 in countries in which the cropland area is below this threshold, whereas the cropland area is maintained at the 2020 level for countries above this threshold. We assumed that first marginal lands and then forests in the expansion of cropland were converted to cropland⁷⁴. We estimated the impact of a higher per capita food demand by adopting the national population in 2020 (ref.⁷⁵) to estimate the total area of croplands based on the per capita cropland area by country for years after 2020, so we took population as a control variable to estimate the impact of increasing per capita food demand on cropland area⁷⁶. We estimated the amount of synthetic N fertilizer applied to the cropland in 167 countries for 1961–2019 by subtracting the amount of synthetic N fertilizer applied to pastures⁵² from the amount of synthetic N fertilizer applied to both pastures and cropland from the FAO dataset of fertilizers⁷⁷. In the future scenarios of intensified N fertilization, we considered that the intensity of N fertilization increases to a specific level (100, 110, ..., 300 kg ha⁻¹) during 2020–2030 in countries in which the intensity is below this threshold, whereas N fertilization is maintained at the 2020 level for countries above this threshold.

Calculation of calories in crops

We calculated the calories in cereal crops based on the production of wheat, rice and maize in the OSCAR model. We estimated the calories in a crop (L) based on the crop yield (Y_i) and the cropland area (A_i):

$$L = \sum_{i=1}^3 \chi A_i Y_i \eta_i (1 - \omega_i) E_i \quad (12)$$

in which i is a crop, χ is the fraction of food loss and waste (56% for developed countries and 44% for developing countries)⁷⁸, η_i is a factor for converting the agricultural product produced to the part that is edible⁷⁹, ω_i is the fraction of crops used for animal feed and other non-food purposes and E_i is the caloric content by weight for each crop. The fraction of crops used for animal feed and other non-food purposes was derived from the FAO global food-balance dataset⁸⁰. Caloric contents were compiled for wheat, rice and maize from the Calories dataset⁸¹. For each country, we considered the calories provided by the animal products compiled from the FAO global food-balance dataset⁷⁵ as a constant, which were added to the calories provided by crops. The parameters χ , η_i , ω_i and E_i by crop are listed in Supplementary Table 6.

Negative emissions from BECCS

We estimated the negative emissions from BECCS based on the quantity of agricultural residues that is harvested from crop production. Negative emissions from BECCS included the reduction in CO₂ emissions by substituting coal to produce the same amount of electricity in power plants and the sequestration of C in biomass to geological repositories¹⁹. We assumed that BECCS was deployed by retrofitting coal-fired power plants. We estimated the negative emissions from BECCS as a function of crop yield (Y_i , g biomass ha⁻¹ year⁻¹) and cropland area (A_i , ha) at an efficiency of C capture and storage of 90%:

$$\Delta E_{\text{BECCS}} = - \left[\sum_{i=1}^8 Y_i A_i \mu_i f_i \frac{(1-l_i)}{l_i} \cdot 90\% + Y_i A_i \mu_i V_i \frac{(1-l_i)}{l_i} \frac{\eta_{\text{bio}}}{V_{\text{coal}} \eta_{\text{coal}}} \xi \right] \quad (13)$$

in which i is a crop (that is, cereals, roots and tubers, beans, oil crops, fibre crops and sugar crops), μ_i is the fraction of dry biomass, f_i is the concentration of C in dry biomass, l_i is the harvest index, defined as the ratio of the mass of the harvested yield to total above-ground biomass, V_i is the ratio of bioenergy to dry biomass (5 MWh (g biomass)⁻¹)⁸², V_{coal} is the energy content of coal (7.44 MWh (g coal)⁻¹)⁸³, ξ is the emission factor of coal (0.67 g C (g coal)⁻¹)⁸⁴ and η_{coal} and η_{bio} are the efficiencies of power generation in coal-fired power plants (39.3%) and BECCS plants (27.8%), respectively⁸⁵. The parameters μ_i , f_i and l_i are listed by crop in Supplementary Table 4.

We assumed that BECCS was used for retrofitting coal-fired power plants (that is, to substitute up to 57%, 83% and 85% of electricity generated by coal in Asia, Europe and North America, respectively, in 2030) before retrofitting oil-fired and gas-fired power plants. We considered four scenarios to examine the impacts of alternative bioenergy applications (Supplementary Fig. 9). First, we considered that BECCS was used for substituting oil or gas rather than coal, in which less emissions were abated owing to a higher power generation efficiency (41% and 47% for oil and gas⁸⁶, respectively, versus 39% for coal⁸⁵) and a lower CO₂ emission factor (0.7 and 0.4 t CO₂ MWh⁻¹ for oil and gas⁸⁷, respectively, versus 0.85 t CO₂ MWh⁻¹ for coal⁸⁴) in power plants. Second, there are technological and market barriers for using bioenergy in transport^{88,89}, which make it difficult to equip CCS on vehicles⁹⁰. We considered a scenario in which biomass produces bioethanol with a 16% energy loss in production⁹¹ to substitute vehicle oils without CCS. Third, we considered a scenario in which the efficiency of energy conversion was increased from 27.8% for BECCS power plants in our central case to 47.5% in biorefinery plants⁴², but 15% of CO₂ released at a high purity during the fermentation process can be captured⁴³. Last, we considered an optimistic scenario in which the efficiency of energy conversion was improved from 27.8% to 47.5% in biorefinery plants, but 55% of CO₂ released during the fermentation process in gasification can be captured at a high purity⁴³.

Our method for estimating the quantity of agricultural residues for BECCS differed from those in previous studies (such as ref.⁹²) based on crop NPP, which scaled as the assumed fraction of agricultural residues that can be harvested in the field. We derived the quantity of agricultural residues from the quantity of the harvested grain using the crop-specified straw-to-grain ratio for above-ground biomass (excluding the difficult-to-obtain biomass, such as roots). The quantity of the collected agricultural residues for bioenergy (q_{straw}) could be computed: $q_{\text{straw}} = x_{\text{straw}} \cdot \eta_{\text{straw}} = [x_{\text{grain}} \cdot (1-l_i)/l_i] \cdot \eta_{\text{straw}} = [q_{\text{grain}}/\eta_{\text{grain}} \cdot (1-l_i)/l_i] \cdot \eta_{\text{straw}} = [q_{\text{grain}} \cdot (1-l_i)/l_i] \cdot (\eta_{\text{straw}}/\eta_{\text{grain}})$, in which x_{straw} is the quantity of agricultural residues from all crops growing in the field, η_{straw} is the fraction of agricultural residues that can be harvested for use as bioenergy, l_i is the harvest index, defined as the ratio of the mass of the harvested grain to total above-ground biomass (Supplementary Table 4), q_{grain} is the quantity of harvested grain and η_{grain} is the fraction of grown grain that can be harvested for food. In the literature, η_{grain} varies from 80% to 95% (refs.^{93,94}) and η_{straw} varies from 83% to 90% (refs.^{95,96}), which both

Article

depend on the locations, type of crop and technology of pretreatment. We considered that the pretreatment of straw can improve η_{straw} (for example, by reducing the volume of straw⁹⁵), whereas the emissions of CO₂ from diesel in the pretreatment estimated in our previous study¹⁹ have been considered in this study. Therefore, we converted the quantity of harvested grain (q_{grain}) to the quantity of harvested residue (q_{straw}) by assuming that it is possible to be equally efficient in harvesting grain and residue. However, this calculation may lead to an upper estimate of the effect of BECCS in mitigation, because sustaining a high η_{straw} for long time may reduce soil fertility and require more fertilizer applications, which deserves attention⁹⁷.

Uncertainty analyses

We estimated the uncertainty in global warming and crop calories by running valid Monte Carlo simulations 1,000 times using the OSCAR model⁹, randomly drawing parameters from their uncertainty distributions⁹⁸. Parameters that varied in the Monte Carlo simulations were: (1) anthropogenic emissions of CO₂, methane and N₂O, LUC emissions of CO₂, emissions of halogenated compounds, ozone precursors (NO_x, CO), VOCs, aerosols (BC, OC, sulfate and nitrate) and aerosol precursors (SO₂, NO_x, O₃, NH₃); (2) natural radiative forcings; (3) parameters governing the processes in oceans, biospheres, wildfires, land uses, hydroxyl groups, wetlands, photolysis, tropospheric ozone, stratospheric ozone, sulfate formation, nitrate formation, secondary organic aerosols, direct and indirect radiative forcings of aerosols, changes in surface albedo, temperature changes, precipitation and ocean acidification; and (4) the fitted coefficients $\alpha^c, \beta^c, \gamma^c, \alpha^t, \beta^t, \gamma^t, \alpha^z$ and γ^z in the relationships between crop yields and atmospheric growing-season temperature, atmospheric CO₂ concentration and intensity of N fertilization. The standard deviations of these fitted coefficients as normal distributions were derived from the regression models, which are listed in Supplementary Table 5. We used the interquartile range and the range of 90% uncertainty from Monte Carlo simulations to indicate the uncertainties in the simulated global warming, crop production and per capita calories.

Data availability

Further material is available in the Supplementary Materials. Code and data used for our analyses are available on the GitHub repository: https://github.com/rongwang-fudan/OSCAR_Agriculture_Global.

55. Li, B. et al. The contribution of China's emissions to global climate forcing. *Nature* **531**, 357–361 (2016).
56. Gasser, T. et al. Path-dependent reductions in CO₂ emission budgets caused by permafrost carbon release. *Nat. Geosci.* **11**, 830–835 (2018).
57. Fu, B. et al. Short-lived climate forcers have long-term climate impacts via the carbon-climate feedback. *Nat. Clim. Change* **10**, 851–855 (2020).
58. Boden, T. A., Andres, R. J. & Marland, G. *Global, Regional, and National Fossil-Fuel CO₂ Emissions (1751–2010) (V. 2013)* https://doi.org/10.3334/CDIAC/O0001_V2013 (Oak Ridge National Laboratory (ORNL), 2013).
59. European Commission, Joint Research Centre/Netherlands Environmental Assessment Agency. *EDGAR - Emissions Database for Global Atmospheric Research, release EDGARv4.2* <http://edgar.jrc.ec.europa.eu/> (2011).
60. Lamarque, J. F. et al. Historical (1850–2000) gridded anthropogenic and biomass burning emissions of reactive gases and aerosols: methodology and application. *Atmos. Chem. Phys.* **10**, 7017–7039 (2010).
61. van der Werf, G. R. et al. Global fire emissions and the contribution of deforestation, savanna, forest, agricultural, and peat fires (1997–2009). *Atmos. Chem. Phys.* **10**, 11707–11735 (2010).
62. Hurtt, G. C. et al. Harmonization of land-use scenarios for the period 1500–2100: 600 years of global gridded annual land-use transitions, wood harvest, and resulting secondary lands. *Clim. Change* **109**, 117–161 (2011).
63. Arora, V. K. et al. Carbon-concentration and carbon-climate feedbacks in CMIP5 Earth system models. *J. Clim.* **26**, 5289–5314 (2013).
64. Li, W., Ciais, P., Makowski, D. & Peng, S. A global yield dataset for major lignocellulosic bioenergy crops based on field measurements. *Sci. Data* **5**, 180169 (2018).
65. Erb, K. H. et al. Unexpectedly large impact of forest management and grazing on global vegetation biomass. *Nature* **553**, 73–76 (2018).
66. Giglio, L., Randerson, J. T. & van der Werf, G. R. Analysis of daily, monthly, and annual burned area using the fourth generation global fire emissions database (GFED4). *J. Geophys. Res.* **118**, 317–328 (2013).

67. Zhou, F. et al. A new high-resolution N₂O emission inventory for China in 2008. *Environ. Sci. Technol.* **48**, 8538–8547 (2014).
68. Davidson, E. A. The contribution of manure and fertilizer nitrogen to atmospheric nitrous oxide since 1860. *Nat. Geosci.* **2**, 659–662 (2009).
69. Hoben, J. P. et al. Nonlinear nitrous oxide (N₂O) response to nitrogen fertilizer in on-farm corn crops of the US Midwest. *Glob. Change Biol.* **17**, 1140–1152 (2010).
70. Prather, M. et al. in *Climate Change 2001: The Scientific Basis: Contribution of Working Group I to the Third Assessment Report of the Intergovernmental Panel on Climate Change* (eds Houghton, J. T. et al.) Ch. 4 (Cambridge Univ. Press, 2001).
71. U.S. Department of Agriculture (USDA). World Agricultural Production (WAP) Circular Dataset <https://ipad.fas.usda.gov/countrysummary/Default.aspx?id=CH&crop=Barley> (2021).
72. Gorelick, N. et al. Google Earth Engine: planetary-scale geospatial analysis for everyone. *Remote Sens. Environ.* **202**, 18–27 (2017).
73. Cai, X., Zhang, X. & Wang, D. Land availability for biofuel production. *Environ. Sci. Technol.* **45**, 334–339 (2011).
74. Bajželj, B. et al. The importance of food demand management for climate mitigation. *Nat. Clim. Change* **4**, 924–929 (2014).
75. Food and Agriculture Organization of the United Nations (FAO). *Annual Population* <https://www.fao.org/faostat/en/#data/OA> (2020).
76. Dawson, I. G. & Johnson, J. E. Does size matter? A study of risk perceptions of global population growth. *Risk Anal.* **37**, 65–81 (2017).
77. Food and Agriculture Organization of the United Nations (FAO). *Fertilizers by Nutrient* <https://www.fao.org/faostat/en/#data/RFN> (2020).
78. Lipinski, B. et al. *Reducing Food Loss and Waste. Working Paper, Installment 2 of "Creating a Sustainable Food Future"* <https://www.wri.org/research/reducing-food-loss-and-waste> (World Resources Institute, 2013).
79. Gustavsson, J., Cederberg, C., Sonesson, U., van Otterdijk, R. & Meybeck, A. *Global Food Losses and Food Waste* <https://www.fao.org/3/mb060e/mb060e00.htm> (Food and Agriculture Organization of the United Nations (FAO), 2011).
80. Food and Agriculture Organization of the United Nations (FAO). *Food Balances (2014–2019)* <https://www.fao.org/faostat/en/#data/FBS> (2020).
81. *Calories.info. Calories in Food: Calorie Chart Database* <https://www.calories.info/> (2021).
82. Kumar, A., Cameron, J. B. & Flynn, P. C. Biomass power cost and optimum plant size in western Canada. *Biomass Bioenergy* **24**, 445–464 (2003).
83. Ghugare, S. B. & Tambe, S. S. Genetic programming based high performing correlations for prediction of higher heating value of coals of different ranks and from diverse geographies. *J. Energy Inst.* **90**, 476–484 (2017).
84. Brander, M., Sood, A., Wylie, C., Haughton, A. & Lovell, J. *Technical Paper | Electricity-specific Emission Factors for Grid Electricity* <https://ecometrica.com/assets/Electricity-specific-emission-factors-for-grid-electricity.pdf> (2011).
85. Shakerl, W., Meerman, H., Talei, A., Ramirez, A. & Faaij, A. Comparative life cycle assessment of biomass co-firing plants with carbon capture and storage. *Appl. Energy* **131**, 441–467 (2014).
86. Graus, W. H. J., Voogt, M. & Worrell, E. International comparison of energy efficiency of fossil power generation. *Energy Policy* **35**, 3936–3951 (2007).
87. RTE France. *eCO₂mix - CO₂ emissions per kWh of electricity generated in France* <https://www.rte-france.com/en/eco2mix/co2-emissions> (2022).
88. Hao, H. et al. Biofuel for vehicle use in China: current status, future potential and policy implications. *Renew. Sustain. Energy Rev.* **82**, 645–653 (2018).
89. Hyrchenko, Y. et al. World market of liquid biofuels: trends, policy and challenges. *E3S Web Conf.* **280**, 05005 (2021).
90. Sharma, S. & Maréchal, F. Carbon dioxide capture from internal combustion engine exhaust using temperature swing adsorption. *Front Energy Res.* **7**, 143 (2019).
91. Ardebili, S. M. S. & Khademalrasoul, A. An analysis of liquid-biofuel production potential from agricultural residues and animal fat (case study: Khuzestan Province). *J. Clean. Product.* **204**, 819–831 (2018).
92. Yang, Y. et al. Quantitative appraisal and potential analysis for primary biomass resources for energy utilization in China. *Renew. Sustain. Energy Rev.* **14**, 3050–3058 (2010).
93. Wolf, J. et al. Biogenic carbon fluxes from global agricultural production and consumption. *Global Biogeochem. Cycles* **29**, 1617–1639 (2015).
94. Gustavsson, J. et al. Food and Agriculture Organization. *Global Food Losses and Food Waste - Extent, Causes and Prevention* (2011).
95. Ji, L. An assessment of agricultural residue resources for liquid biofuel production in China. *Renew. Sustain. Energy Rev.* **44**, 561–575 (2015).
96. Gao, J. et al. An integrated assessment of the potential of agricultural and forestry residues for energy production in China. *Glob. Change Biol. Bioenergy* **8**, 880–893 (2016).
97. Zhao, G. et al. Sustainable limits to crop residue harvest for bioenergy: maintaining soil carbon in Australia's agricultural lands. *Glob. Change Biol. Bioenergy* **7**, 479–487 (2015).
98. Sokal, R. R. & Rohlf, F. J. *Biometry: The Principles and Practice of Statistics in Biological Research* (W. H. Freeman, 1981).

Acknowledgements R.W. appreciates the provision of funds from the National Natural Science Foundation of China (41877506) and the Chinese Thousand Youth Talents Program. R.Z., X.T., J. Chen and R.W. acknowledge support from the Shanghai International Science and Technology Partnership Project (21230780200). X.T. and R.W. acknowledge support from the Fudan-Sinar Mas Think Tank Fund (JGSXK2014). P.C. acknowledges support from the ANR CLAND Convergence Institute 16-CONV-0003. J.P. and J.S. acknowledge the financial support from the Catalan Government grants SGR 2017-1005 and AGAUR-2020PANDE00117, the Spanish Government grant PID2019-110521GB-I00 and the Fundación Ramón Areces grant ELEMENTAL-CLIMATE. T.G. acknowledges support from the Austrian Science Fund (FWF) under grant agreement P31796-N29 (ERM project).

Author contributions R.W. conceived the research, designed the study and wrote the first version of manuscript. S.X. compiled data, performed the research and prepared graphs. T.G. provided the OSCAR model. P.C., T.G., J.P., Y.B., O.B., I.A.J., J.S., J.H.C., J. Cao and R.Z. provided

tools analysing the relationship between climate change and food security. J.P., P.C., I.A.J. and J.S. provided tools analysing the ecological impact of using bioenergy. J.H.C. and X.F.X. provided tools analysing the measures of using green energy. J. Cao, J. Chen, L.W., X.T. and R.Z. provided tools analysing the impact of climate change on the agronomy. All co-authors interpreted the results and contributed to the writing.

Competing interests The authors declare no competing interests.

Additional information

Supplementary information The online version contains supplementary material available at <https://doi.org/10.1038/s41586-022-05055-8>.

Correspondence and requests for materials should be addressed to Rong Wang.

Peer review information *Nature* thanks Gernot Wagner and the other, anonymous, reviewer(s) for their contribution to the peer review of this work. Peer reviewer reports are available.

Reprints and permissions information is available at <http://www.nature.com/reprints>.